Kinetic and Thermodynamic Characterization of the Common Polymorphic Variants of Human Methionine Synthase Reductase†

Horatiu Olteanu,‡,§ Kirsten R. Wolthers,|| Andrew W. Munro,|| Nigel S. Scrutton,*,|| and Ruma Banerjee*,‡

Department of Biochemistry, University of Nebraska, Lincoln, Nebraska 68588-0664, and Department of Biochemistry, University of Leicester, University Road, Leicester LE1 7RH, U.K.

Received October 27, 2003; Revised Manuscript Received December 17, 2003

ABSTRACT: Human methionine synthase reductase (MSR) is a protein containing both FAD and FMN, and it reactivates methionine synthase that has lost activity due to oxidation of cob(I)alamin to cob(II)alamin. In this study, anaerobic redox titrations were employed to determine the midpoint reduction potentials for the flavin cofactors in two highly prevalent polymorphic variants of MSR, I22/L175 and M22/S175. The latter is a genetic determinant of plasma homocysteine levels and has been linked to premature coronary artery disease, Down's syndrome, and neural tube defects. The I22/L175 polymorphism has been described in a homocystinuric patient. Interestingly, this polymorphism is in the extended linker region between the two flavin domains, which may mediate or facilitate interaction with methionine synthase. In MSR I22/L175, the FMN potentials are −103 mV (oxidized/semiquinone) and −175 mV (semiquinone/hydroquinone) at pH 7.0 and 25 °C, and the corresponding FAD potentials are −252 and −285 mV, respectively. For the M22/S175 variants, the values of the four midpoint potentials are −114 mV (FMN oxidized/semiquinone), −212 mV (FMN semiquinone/hydroquinone), −236 mV (FAD oxidized/semiquinone), and −264 mV (FAD semiquinone/hydroquinone). The midpoint potential values in the two variants are generally comparable to those originally determined for the MSR I22/S175 variant [Wolthers, K. R. (2003) *Biochemistry 42,* 3911−3920], with relatively minor variations in the different redox couples. In each case, blue neutral flavin semiquinone species are stabilized on both flavins, and are characterized by a broad absorption band in the long wavelength region. In addition, stopped-flow absorption and fluorescence spectroscopy were used to study the pre-steady state reduction kinetics by NADPH of the two polymorphic variants. The reversible kinetic model proposed for wild-type MSR was validated for the I22/L175 and M22/S175 variants. Thus, the biochemical penalties associated with these polymorphisms, which result in less effective methionine synthase activation, do not appear to result from differences in their reduction kinetics. It is likely that differences in their relative affinities for the redox partner, methionine synthase, underlie the differences in the relative efficiencies of reductive activation exhibited by the variants.

Methionine synthase reductase (MSR) is an enzyme containing both FAD and FMN, and it is involved in regenerating the activity of mammalian cobalamin-dependent methionine synthase (*1*, *2*). The reductive activation involves conversion of cob(II)alamin, which occasionally forms from oxidation of cob(I)alamin during catalysis by methionine synthase, to methylcobalamin. Formation of the latter from cob(II)alamin restores the active state of methionine synthase and thus maintains the metabolic pathway that salvages homocysteine as methionine.

MSR is similar to cytochrome P450 reductase, the first recognized member of the family of enzymes that contains both FMN and FAD (*3*). This family includes the eukaryotic members NOS (*4*, *5*) and NR1 (*6*), as well as prokaryotic members such as the flavocytochrome P450 BM3 (*7*), and sulfite reductase (*8*). The fact that the acceptor substrate for these enzymes is a protein is a hallmark of this enzyme family. These enzymes seem to have evolved phylogenetically by the fusion of two ancestral genes, one that encodes an FMN-containing flavodoxin and the other an FAD-containing ferredoxin oxidoreductase (*9*, *10*). The combination of the two flavins on a unique protein scaffold ensures the proximity required for efficient electron transfer between cofactors, and presumably fine-tunes the thermodynamic and kinetic properties of internal electron transfer through a relatively flexible linker of variable length.

Patients belonging to the *cbl*E complementation group of functional methionine synthase deficiency have a genetic defect associated with MSR, which is inherited as an autosomal recessive disorder (*11*−*13*). MSR mutations described in both the flavin-binding regions and the con-

† This work was supported by grants from the National Institutes of Health (DK64959 and DK45776 to R.B. and a postdoctoral fellowship to K.R.W.) and by a predoctoral fellowship from the American Heart Association to H.O. N.S.S. is a Lister Institute Research Professor. R.B. is an Established Investigator of the American Heart Association.

* To whom correspondence should be addressed. R.B.: e-mail, rbanerjee1@unl.edu; telephone, (402) 472-2941. N.S.S.: e-mail, nss4@le.ac.uk; telephone, +44 116 223 1337.

‡ University of Nebraska.

§ Current address: Department of Pathology, University of Texas Southwestern Medical Center, Dallas, TX 75235.

|| University of Leicester.

10.1021/bi035910i CCC: $27.50 © 2004 American Chemical Society
Published on Web 01/29/2004

necting spacer domain (*2*, *14*) are related to a severe clinical picture accompanying the manifestations of classical hyperhomocysteinemia (*15*, *16*). From an epidemiologic point of view, it is also important to focus on genetic polymorphisms that may potentially induce mild hyperhomocysteinemia and, in turn, could enhance the risk of degenerative afflictions such as atherosclerotic vascular modifications (*17*, *18*) or other organ system disorders, including neural tube defects (*19*) and Down's syndrome (*19*, *20*). To date, two polymorphisms identified in the MSR open reading frame have received particular attention, namely, I22M (*18*, *21*, *22*) and S175L. Particular emphasis was put on the study of the I22M variant, which was the first one to be associated with an allele frequency of ~0.55 for isoleucine (*18*, *21*, *22*). It was the key player in several genetic studies of homocysteine-related conditions, viz., premature cardiopathy, spina bifida, and trisomy 21 (*17*−*22*), and was reported to be a genetic determinant of increased blood homocysteine levels (*18*). In contrast, the S175L polymorphism is less well studied, and to our knowledge, there is only one report describing the presence of this variant in a *cbl*E patient and the prevalence in a group of healthy subjects [allele frequency for serine of 0.62 (*23*)]. Our early efforts were dedicated to understanding the spectral and kinetic characteristics of the M22/S175 and I22/L175 recombinant MSR proteins and to compare those properties with those of the I22/S175 ("wild-type") counterpart (*24*). We noticed a difference in the efficiency of their electron transfer to the natural substrate, methionine synthase, and to a series of artificial electron acceptors. These results were interpreted in terms of a diminished affinity between the MSR variants and methionine synthase. Although the redox potentials for the flavins in wild-type I22/S175 MSR have been reported (*25*), these values were unknown for the variants.

In this study, we compare the thermodynamic and kinetic properties of the M22/S175 and I22/L175 variants in detail to assess how these polymorphisms affect the properties of MSR. The findings of an altered biochemical phenotype may help us understand the potential influence of a suboptimal methionine synthase activity on homocysteine blood concentration and homocysteine-related disease in individuals harboring these polymorphisms. These studies demonstrate that the common polymorphisms, I22M and S175L, do not influence the redox centers in the protein to the extent where there should be any major influence on turnover with methionine synthase (an overview of the redox potential values is presented in Tables 1 and 2 and Figure 9). They are consistent with our previous finding that the biochemical phenotypes of the polymorphic variants appear to result from altered affinities for the redox partner, methionine synthase. The polymorphisms presumably exert only a mild effect on homocysteine metabolism *in vivo*, which is to be expected, considering the common occurrence of the I22M and S175L substitutions in healthy human subjects (*21*, *23*).

EXPERIMENTAL PROCEDURES

Chemicals and Reagents. Glutathione Sepharose 4B was purchased from Amersham Pharmacia (Piscataway, NJ). Complete protease inhibitor tablets were from Roche (Indianapolis, IN), and all other chemicals were from Sigma (St. Louis, MO).

Expression and Purification of Human Methionine Synthase Reductase Variants. The MSR polymorphic variants, M22/S175 and I22/L175, were expressed as GST fusion proteins in *Escherichia coli* strain BL21(DE3), using a modified version of the protocol described previously (*1*). Briefly, an overnight culture of *E. coli* containing the appropriate expression construct was grown at 37 °C in LB medium containing ampicillin (100 μg/mL). One liter of modified Terrific Broth (20 g of yeast extract, 10 g of bactotryptone, 4 mL of glycerol, 4.33 g of Na_2HPO_4, and 2.65 g of KH_2PO_4), with 100 μg/mL ampicillin, was inoculated with 10 mL of overnight culture and grown in a shaker at 28 °C. When the culture reached an OD_{600} of ~1.0, IPTG was added to a final concentration of 0.1 mM and the temperature was lowered to 25 °C. The cells were grown further overnight, pelleted by centrifugation at 5000*g* for 20 min, and stored at −80 °C until they were used further.

The frozen cells were thawed and resuspended in GST wash/bind buffer (4.3 mM Na_2HPO_4, 1.47 mM KH_2PO_4, 137 mM NaCl, 2.7 mM KCl, 0.5 mM EDTA, and 1 mM DTT containing Complete protease inhibitor tablets). Cell lysis was achieved by addition of lysozyme (200 μg/mL) and sonication (seven 20 s bursts with 3 min pause intervals at a power setting of 7), using a Misonix XL2020 sonicator (Misonix Inc.). The sonicate was centrifuged at 15000*g* for 60 min to pellet cell debris and insoluble matter. The resulting supernatant was loaded on a Glutathione Sepharose 4B column, previously equilibrated with GST wash/bind buffer. Nonspecifically bound proteins were washed from the column with 1 L of GST wash/bind buffer, and the GST-fused MSR variant proteins were eluted with a 10 mM GSH solution in 50 mM Tris-HCl (pH 8.0), 0.5 mM EDTA, and 1 mM DTT. The GST tag was removed by limited proteolysis with thrombin. The buffer was exchanged with 50 mM potassium phosphate buffer (pH 7.0) by overnight dialysis of MSR at 4 °C, and the enzyme was further purified by anion exchange chromatography as previously described (*1*). The concentration of purified recombinant MSR was determined spectroscopically, using a molar extinction coefficient of 21 600 M^{-1} cm^{-1} at 450 nm. Approximately 8 mg of MSR M22/S175 or I22/L175 was obtained per liter of culture.

Potentiometric Titrations. Redox titrations were performed anaerobically in a Belle Technology glovebox, under a nitrogen atmosphere at 25 °C. Oxygen levels were maintained at less than 5 ppm. Titrations were performed in 100 mM potassium phosphate buffer (pH 7.0) made anaerobic by argon bubbling. Concentrated protein samples (100 μM in a total volume of 1−2 mL) were treated with several crystals of potassium ferricyanide to ensure full oxidation and then were admitted to the glovebox. The protein was then made oxygen-free by passing it over a 10 mL Econo-Pac 10 DG column (Bio-Rad, Hercules, CA), pre-equilibrated with anaerobic titration buffer [100 mM potassium phosphate (pH 7.0)]. This step was also used to remove excess ferricyanide. The eluted protein sample was diluted with titration buffer to a total volume of 8 mL (25 μM MSR based on flavin content, final concentration). Prior to titration, redox mediators were added to the protein solution, to mediate electrical communication between the electrode and enzyme. Typical mediator concentrations were as follows: 5 μM 2-hydroxy-1,4-naphthoquinone, 2 μM phenazine methosulfate, 1 μM benzyl viologen, and 0.5 μM methyl viologen.

All of these mediators were mixed together for individual experiments. Absorption spectra (250−800 nm) were collected using a fiber optic absorption probe (Varian) connected to a Varian Cary 50Bio UV−visible spectrophotometer. The electrochemical potential of the solution was measured using a Pt/Calomel electrode (ThermoRussel Ltd.) linked to a Hanna pH211 pH/voltmeter. The electrode was calibrated using the Fe(II)/Fe(III)/EDTA couple (108 mV) as a standard, and the measured potentials were normalized relative to the standard hydrogen electrode by a factor of 244 mV. The oxidized protein solutions were initially titrated electrochemically with sodium dithionite as a reductant and then reoxidized with potassium ferricyanide according to the method of Dutton (*26*). Aliquots of either dithionite or ferricyanide were delivered from concentrated stock solutions, and absorbance spectra of the protein were recorded after each addition, once the potential values were allowed sufficient time to stabilize. Typical experiments required the collection of 60−90 spectra at various potentials. During the several hours required to complete a full titration of MSR, a small amount of baseline drift occurred, causing minor increases in the absorbance across the entire spectrum. To correct for these changes (typically ∼0.05 absorbance unit), small corrections were made to restore the absorption at 800 nm to zero in all spectra.

All data manipulations and analysis were performed using Origin version 6 or 7 (MicroCal). From the set of spectra obtained during titration experiments, the absorbance values of the flavin cofactors at different wavelengths were plotted against potential, to determine the redox potentials for FAD and FMN. The absorbance values between 450−460 nm (λ_{max} for oxidized flavin) and 580−605 nm (λ_{max} for the blue semiquinone flavin) were summed and used for the analysis of titration data. In addition, the isosbestic point at 500 nm, associated with the $E_{ox}-E_{sq}$ transition, and the isosbestic point at 425 nm, associated with the latter half of the $E_{sq}-E_{red}$ transition, were also plotted versus potential. The 425 and 500 nm plots were fitted to eq 1, which describes a two-electron reduction process and is derived by extension of the single-electron Nernst equation and the Lambert−Beer law (*26*, *27*):

$$A = \frac{a \times 10^{(E-E'_1)/59} + b + c \times 10^{(E'_2-E)/59}}{1 + 10^{(E-E'_1)/59} + 10^{(E'_2-E)/59}} \quad (1)$$

The 450−460 and 580−605 nm plots were fitted to eq 2, which represents the sum of two two-electron redox processes:

$$A = \frac{a\,10^{(E-E'_1)/59} + b + c \times 10^{(E'_2-E)/59}}{1 + 10^{(E-E'_1)/59} + 10^{(E'_2-E)/59}} + \frac{d \times 10^{(E-E'_3)/59} + e + f \times 10^{(E'_4-E)/59}}{1 + 10^{(E-E'_3)/59} + 10^{(E'_4-E)/59}} \quad (2)$$

In these equations, A is the total absorbance, a, b, and c are absorbance values contributed by one of the flavins in the oxidized, semiquinone, and hydroquinone oxidation states, respectively, while d, e, and f are the corresponding absorbance components associated with the second flavin, E is the observed potential, E'_1 and E'_2 are the midpoint potentials for the first flavin, corresponding to the oxidized/semiquinone and semiquinone/hydroquinone couples, respectively, and E'_3 and E'_4 are the corresponding midpoint potentials of the second flavin.

The data fitted to eq 1 by nonlinear least-squares regression analysis provided values for the midpoint potentials of the oxidized/semiquinone and semiquinone/hydroquinone couples of the individual flavin cofactors. During this process, the variables were unconstrained and regression analysis provided values in close agreement to those of the initial estimates. However, because of the large number of parameters in fitting eq 2, estimates of the potential values ($E'_1-E'_4$) obtained from the previous two-electron fits were used. Also, estimates of the values of the absorbance components needed to be made to prevent unrealistic fitting. The first several iterations had the potential values fixed. Then, the absorbance values were fixed and the potential values allowed to vary during the fitting routine. By alternating these processes several times, we obtained reasonable values for the absorbances and potentials, with only the redox potentials being allowed to vary during the final fitting cycle.

Kinetic Measurements. Stopped-flow studies were performed using an Applied Photophysics SX.17 MV stopped-flow spectrophotometer. Unless otherwise stated, measurements were taken at 25 °C in 50 mM potassium phosphate buffer (pH 7.0). The protein concentration was 10 μM for single-wavelength and 25 μM for multiple-wavelength absorption studies (reaction cell concentration), and reactions were performed under anaerobic conditions. For this purpose, the sample handling unit of the stopped-flow instrument was contained within a glovebox (Belle Technology). All buffers were made anaerobic by extensive bubbling with argon before use. Prior to stopped-flow studies, protein samples were treated with potassium ferricyanide, and excess ferricyanide was removed by rapid gel filtration on Econo-Pac 10 DG columns (Bio-Rad) equilibrated in 50 mM potassium phosphate buffer (pH 7.0).

Stopped-flow multiwavelength absorption studies were carried out using a photodiode array detector and X-SCAN software (Applied Photophysics Ltd., Surrey, U.K.). Spectral deconvolution was performed by singular-value decomposition (SVD) methods using PROKIN software (Applied Photophysics Ltd.). In single-wavelength studies, flavin reduction by NADPH in the MSR polymorphic variants was observed at 454 nm. Transients were biphasic (over 10 s) and were fitted using the standard double-exponential expression (eq 3):

$$A = C_1 e^{-k_{obs1}t} + C_2 e^{-k_{obs2}t} + b \quad (3)$$

where k_{obs1} and k_{obs2} are the observed rate constants for the fast and slow phases, respectively, C_1 and C_2 are the relative amplitude values for the two phases, and b is the offset corresponding to a non-zero baseline value. NADPH reduction of MSR analyzed by photodiode array studies resulted in a reverse rate for flavin reduction that is several orders of magnitude slower than the forward reaction. Therefore, simplified hyperbolic eq 4 was used to describe the NADPH concentration dependence of k_{lim} (the limiting rate of flavin reduction).

$$k_{obs} = \frac{k_{lim}[S]}{K + [S]} \quad (4)$$

where [S] is the NADPH concentration and K is the substrate concentration at the $k_{lim}/2$ value.

Stopped-flow absorbance traces detected at 600 nm described the generation and subsequent decay of an NADPH-oxidized enzyme charge transfer species and consisted of a rapid "up" followed by a slower "down" phase. Equation 5 was used to fit the observed rates for these two phases:

$$A = \frac{k_{obs1}}{k_{obs2} - k_{obs1}}(C_1 e^{-k_{obs1}t} - C_2^{-k_{obs2}t}) + b \qquad (5)$$

where k_{obs1} and k_{obs2} are the observed rate constants for the appearance and decay of the charge transfer intermediate, respectively, C_1 and C_2 are the corresponding amplitude terms, and b is the offset value.

An excitation wavelength of 295 nm was employed for stopped-flow tryptophan fluorescence experiments. The emission wavelength (340 nm) was selected using the appropriate band-pass filter. Data fitting to fluorescence transients was done by using a standard monophasic equation.

RESULTS

Redox Titrations of the MSR I22/L175 and M22/S175 Polymorphic Variants. The general changes in the spectral properties of the two polymorphic variants were very similar during the course of electrochemical redox titrations. Therefore, the results with only one, MSR I22/L175, are described here in detail. Anaerobic spectroelectrochemical titration experiments allowed determination of the four midpoint potentials for reduction of the two flavins. Titrations proceeded from the fully oxidized enzyme form, which was gradually reduced by adding small aliquots of a concentrated sodium dithionite stock solution. The fully reduced enzyme was then reoxidized by addition of aliquots from a stock solution of potassium ferricyanide. A stable voltage reading indicated full equilibration after each addition of reducing or oxidizing agent. Similar spectra were recorded at essentially identical potential values during the reductive and oxidative titrations, suggesting the absence of hysteretical behavior during the experiments.

The MSR protein remained generally stable upon reduction by dithionite, which allowed a high-quality set of spectra to be recorded. Minor spectral drifts were corrected by simple baseline subtraction, as described in Experimental Procedures. Figure 1 shows a typical set of corrected spectral traces obtained during redox titration of MSR I22/L175. The reduction process can be dissected into three distinct phases. In the first phase of the titration (solid lines in Figure 1), addition of dithionite results in accumulation of the blue semiquinone species, as indicated by the broad absorbance band centered at 595 nm. An isosbestic point evident in this phase of the titration is attributed to the FMN_{ox}−FMN_{sq} transition (a reduction potential more positive than −130 mV). In the first part of the second phase of the titration (potential values between approximately −130 and − 180 mV), the absorption of the semiquinone species stays close to its maximal value, concomitant with a decrease in absorbance of the lower-wavelength absorbance peaks. Between approximately −180 and −270 mV, the semiquinone signal decays considerably. Spectra in the region between −130 and −270 mV are represented with dotted lines. No obvious isosbestic points are visible during this phase of titration, because of the presence of multiple partially reduced forms of MSR, i.e., FMN_{sq}/FAD_{ox}, FMN_{sq}/FAD_{sq}, and FMN_{hq}/FAD_{sq}. At potentials more negative than approximately −270 mV, the third and final phase of the titration is observed (dashed lines). In this phase, the major observed spectral change is due to reduction of the FAD blue semiquinone to the hydroquinone species. An isosbestic point is seen at 425 nm during this phase, due to the predominance of only two species (FAD_{sq} and FAD_{hq}) as the titration approaches completion.

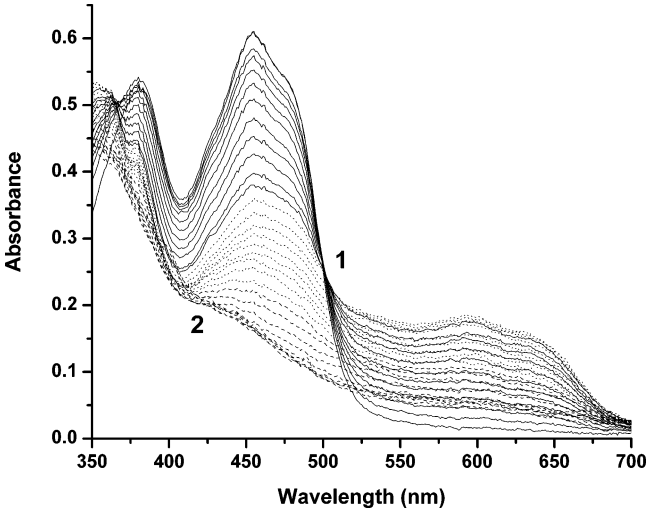

FIGURE 1: Absorption spectra for the redox titration of MSR I22/L175 (25 μM). The spectra were recorded after each addition of dithionite as described in Experimental Procedures. The solid lines represent spectra recorded during the addition of the first equivalent and are characteristic of the oxidized−semiquinone transition of the flavins. An isosbestic point at 500 nm appearing during this transition is labeled with a 1. The dotted lines represent spectra recorded between potential values of approximately −130 and −270 mV. The dashed lines represent spectra at potentials more negative than −270 mV. During this phase of the titration, an isosbestic point (labeled with a 2) appears at 425 nm.

A plot of the summed absorbance values from 450 to 460 nm (spanning the oxidized flavin absorbance maximum) versus potential is shown in Figure 2A. The redox profile is composed of two sigmoidal features that merge at approximately −150 mV. From previous potentiometric analyses of related FAD- and FMN-containing enzymes (*27*), the positive end of the trace is ascribed to the FMN_{ox}/FMN_{sq} couple, whereas the remaining components (at the negative end) are a function of the other three midpoint potentials: FAD_{ox}/FAD_{sq}, FAD_{sq}/FAD_{hq}, and FMN_{sq}/FMN_{hq}. Compared to wild-type MSR (I22/S175), the redox titration plot reveals a smaller separation between the FMN_{ox}/FMN_{sq} potential and the three remaining redox couples for the MSR I22/L175 and M22/S175 variants (72 and 98 mV separate the FMN_{ox}/FMN_{sq} and FMN_{sq}/FMN_{hq} couples, respectively, compared with 118 mV in the wild type). Both CPR (*27*) and NOS (*28*) have much larger separations between these couples than wild-type MSR. However, only for the MSR I22/L175 does the midpoint potential for the two-electron reduction of the FMN (−139 mV) vary significantly from that for the wild type (−168 mV) or the M22/S175 variant (−163 mV). The dependence of the summed absorbances between 580 and 605 nm (across the blue semiquinone maxima) is shown in

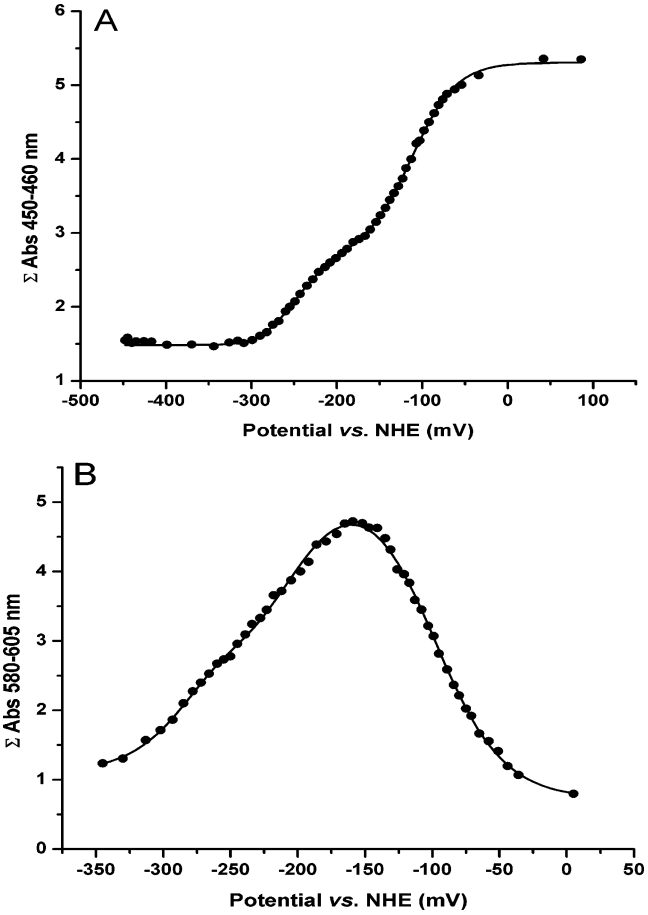

FIGURE 2: Plots of absorbance vs potential for MSR I22/L175. In panel A, the sum of absorbance values between 450 and 460 nm is plotted against the reduction potential. In panel B, the summed absorbance values between 580 and 605 nm are plotted against the potential. Both data sets were fitted to eq 2 as described in Experimental Procedures, and the midpoint potentials for the oxidized/semiquinone and semiquinone/hydroquinone couples of both flavins are given in Table 1. The corresponding data for the M22/S175 variant are given in Table 2.

Figure 2B for MSR I22/L175. The bell-shaped curve includes two semiquinone signals, with the high-potential FMN_{ox}/FMN_{sq} couple in the right-hand region and the three remaining midpoint potentials on the left-hand side of the curve. The features of this plot mirror those seen with wild-type MSR I22/S175 and differ from the distinctly asymmetrical bell-shaped trace found in CPR (*27*) and NOS (*28*). For the MSR I22/L175 variant, a slight asymmetry can be discerned in the lower limb of the curve, with a minor inflection seen at approximately −250 mV. A slightly more pronounced inflection at the same position is observed for the M22/S175 variant (data not shown), due to small changes in the relative potentials for the FMN_{sq}/FMN_{hq}, FAD_{ox}/FAD_{sq}, and FAD_{sq}/FAD_{hq} couples for this mutant.

Analysis of the data from these two plots allows the calculation of the contributing midpoint potentials (two oxidized/semiquinone and two semiquinone/hydroquinone) by using eq 2, which relates the changes in absorbance and potentials to a four-electron reduction process. Because of the relatively large number of parameters that are involved, it was necessary to impose several constraints for the amplitude of the contributing absorbance coefficients, as described in Experimental Procedures. In this way, reasonable estimates of the midpoint potentials are obtained and their validity is supported by the generally good agreement in the values obtained from the two four-electron plots for both the MSR I22/L175 and M22/S175 variants (Tables 1 and 2). The differences in values calculated from the data at 450 and 590 nm are due to variations in the algorithm fitting to each individual data set.

Table 1: Reduction Potentials for the Flavin Cofactors in MSR I22/L175

	reduction potential (mV) vs a normal hydrogen electrode			
	FMN cofactor		FAD cofactor	
	ox/sq	sq/red	ox/sq	sq/red
425 nm[a]	−104 ± 3	−	−248 ± 5	−
500 nm[a]	−	−185 ± 4	−	−262 ± 5
450−460 nm[b]	−103 ± 4	−175 ± 4	−252 ± 4	−285 ± 6
580−605 nm[b]	−99 ± 3	−208 ± 5	−246 ± 6	−270 ± 4

[a] Values are from a fit of the data shown in Figure 3 to eq 1. [b] Values are from a fit of the data shown in Figure 2 to eq 2. The errors are from nonlinear least-squares fits of the data shown in the corresponding figure.

Table 2: Reduction Potentials for the Flavin Cofactors in MSR M22/S175

	reduction potential (mV) vs a normal hydrogen electrode			
	FMN cofactor		FAD cofactor	
	ox/sq	sq/red	ox/sq	sq/red
425 nm[a]	−117 ± 4	−	−245 ± 6	−
500 nm[a]	−	−217 ± 5	−	−286 ± 8
450−460 nm[b]	−114 ± 4	−212 ± 10	−236 ± 5	−264 ± 6
580−605 nm[b]	−104 ± 5	−212 ± 5	−244 ± 4	−273 ± 7

[a] Values are from the isosbestic points data vs potential, fitted to eq 1. [b] Values are from the absorbance (450−460 and 580−605 nm, respectively) data vs potential, fitted to eq 2. The errors are from nonlinear least-squares fits of the data generated in one experiment.

The potentials of the individual redox couples can be further cross-checked against the results derived from analysis of the absorbance versus potential data at the two isosbestic points, 425 and 500 nm, respectively (Figure 3). At an isosbestic wavelength, there is near-zero absorbance variation accompanying the electronic transition of a redox couple, e.g., the semiquinone−hydroquinone transition in the case of the 425 nm isosbestic point. Hence, plotting the absorbance change at this wavelength (425 nm) versus the potential can be used to extract the midpoint potentials for the oxidized/semiquinone couples of both FMN and FAD. Conversely, analysis of the absorbance at 500 nm versus potential will yield the midpoint potentials for the semiquinone/hydroquinone couples for each of the flavins. Equation 1 was used to fit the data in panels A and B of Figure 3, and the resulting midpoint potential values were obtained: −104 mV for FMN_{ox}/FMN_{sq}, −185 mV for FMN_{sq}/FMN_{hq}, −248 mV for FAD_{ox}/FAD_{sq}, and −262 mV for FAD_{sq}/FAD_{hq} (Table 1). The values of the midpoint potentials determined by either the two-electron or four-electron approaches were in good agreement for MSR I22/L175 and underscore the validity of the analytical methods that were employed. When compared to that of the wild-type MSR I22/S175, the only difference of note is the aforementioned decrease in potential difference between the

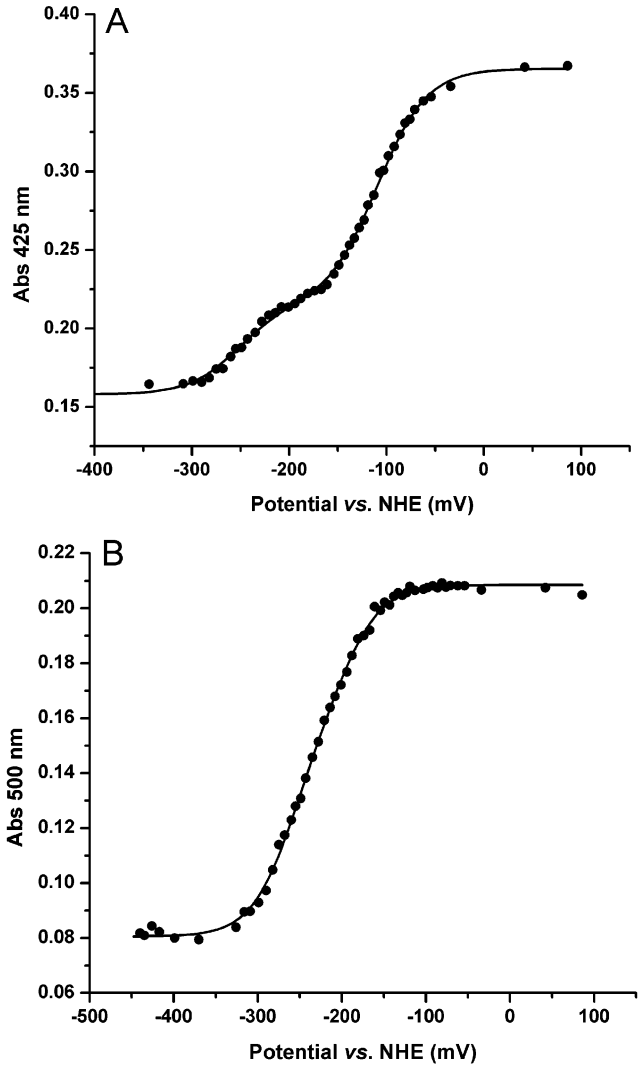

FIGURE 3: Plots of absorbance vs potential for MSR I22/L175 at isosbestic points shown in Figure 1. In panel A, the absorbance at 425 nm (isosbestic point for the semiquinone/hydroquinone couples of both flavins) is plotted against the potential. In panel B, the absorbance at 500 nm (isosbestic point for the oxidized/semiquinone couples of both flavins) is plotted against the potential. The data were fitted to eq 1 as described in Experimental Procedures, and the midpoint potentials for all four couples are given in Table 1. The corresponding data for the M22/S175 variant are given in Table 2.

FMN_{ox}/FMN_{sq} and FMN_{sq}/FMN_{hq} couples. Otherwise, the relatively small alterations in the potentials suggest no major change in the electron transfer properties of this polymorphic variant.

The electrochemical titrations of the MSR M22/S175 polymorphic variant yielded similar spectral changes as shown in Figure 4, and were analyzed using the same set of approaches as described for the other variant (Table 2). The redox potential values are in close agreement for the two variants, with the M22/S175 variant being rather more similar to the wild-type MSR due to the more similar potential values of the FMN cofactor.

Flavin Reduction Monitored by Photodiode Array Spectroscopy. The reductive half-reaction of the MSR polymorphic variants was initially investigated at 25 °C under pseudo-first-order conditions (20-fold excess of NADPH). Rapid mixing of MSR (either I22/L175 or M22/S175) with NADPH

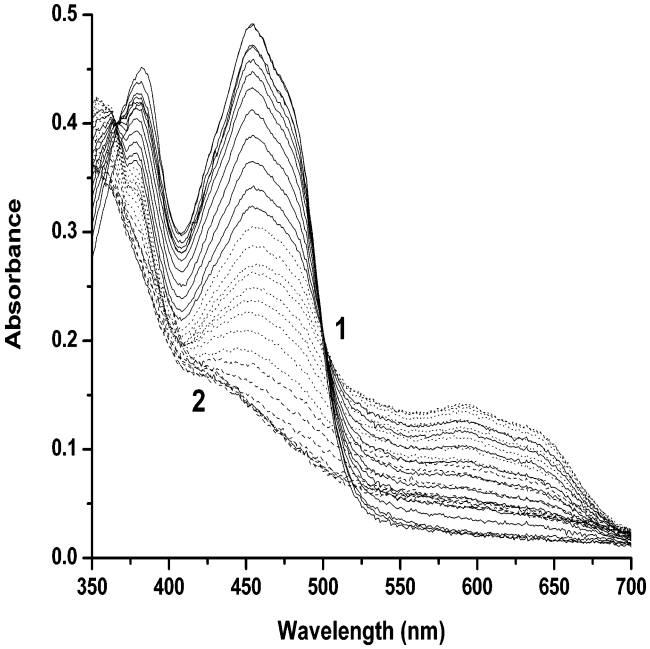

FIGURE 4: Absorption spectra for the redox titration of MSR M22/S175 (20 μM). The spectra were collected after each addition of dithionite as described in Experimental Procedures. The solid lines represent spectra recorded during the addition of the first electron, following the oxidized−semiquinone transition of the flavins. An isosbestic point at 500 nm appearing during this transition is labeled with a 1. The dotted lines represent spectra recorded between potential values of approximately −130 and −270 mV. The dashed lines represent spectra at potentials more negative than −270 mV. During this phase of titration, an isosbestic point (labeled with a 2) appears at 425 nm.

was followed for 200 s, during which time enzyme reduction occurred, as noticed by the progressive reduction of the magnitude of the absorption peak at 454 nm. Since the spectral data for the two variants were virtually identical, only those of the I22/L175 variant are shown (Figure 5A). Spectra collected during this time interval were globally fitted by SVD analysis to a three-step reversible model, involving four discrete spectral species (Figure 5B). The observed kinetic rates for the two MSR variants are comparable and virtually identical to those generated with the wild-type enzyme (*29*) (Table 3). Hence, a reaction scheme described by a three-step model (Scheme 1) fits the data well with respect to both the rates and the absorbance values of the intermediates previously ascribed to wild-type MSR (*29*). Briefly, these steps are (i) conversion of oxidized enzyme A to FAD hydroquinone species B followed by (ii) an equilibrium of two-electron-reduced enzyme populations, comprising FAD_{hq}/FMN_{ox}, FAD_{sq}/FMN_{sq}, and FAD_{ox}/FMN_{hq} couples and (iii) the formation of the four-electron-reduced enzyme species upon transfer of an electron from a second molecule of NADPH.

Single-Wavelength Absorption and Fluorescence Studies. Single-wavelength stopped-flow studies were performed to determine rate constants for the formation of spectral intermediates seen in the photodiode array experiments. In addition, they substantiated the assignment of kinetic phases in the global fitting model. Transients measured at 454 nm under pseudo-first-order conditions (rapid mixing of MSR I22/L175 or MSR M22/S175 with an at least 20-fold excess NADPH) were best described by a biphasic exponential equation (over 10 s), and the data for the I22/L175 variant

Table 3: Comparison of Kinetic Rate Constants in Wild-Type MSR and MSR Polymorphic Variants

	rate constant (s^{-1})		
	MSR I22/S175[a]	MSR I22/L175[b]	MSR M22/S175[c]
A → B	24.9 ± 0.1	16.3 ± 0.05	16.7 ± 0.03
B → A	$(3.2 \pm 1.4) \times 10^{-4}$	$(9.9 \pm 2.5) \times 10^{-4}$	$(1.8 \pm 0.1) \times 10^{-4}$
B → C	0.18 ± 0.00	0.15 ± 0.00	0.14 ± 0.00
C → B	$(1.7 \pm 0.1) \times 10^{-3}$	$(1.9 \pm 0.2) \times 10^{-3}$	$(1.5 \pm 0.5) \times 10^{-5}$
C → D	$1.6 \times 10^{-2} \pm 0.03 \times 10^{-3}$	$(1.3 \pm 0.01) \times 10^{-2}$	$(1.3 \pm 0.01) \times 10^{-2}$
D → C	$(1.1 \pm 0.1) \times 10^{-4}$	$(3.8 \pm 0.8) \times 10^{-4}$	$(2.9 \pm 0.2) \times 10^{-4}$
k_{lim} (454 nm)	24.8 ± 0.3	21.5 ± 0.2	20.5 ± 0.2
K (μM)	57.2 ± 2.6	91.0 ± 3.1	74.4 ± 2.9

[a] Values from ref *29*. [b] Values are from the data depicted in Figures 5B (global fit) and 6B (fitted to eq 5). [c] Values are from multiple-wavelength and single-wavelength (454 nm) absorption experiments (data not shown).

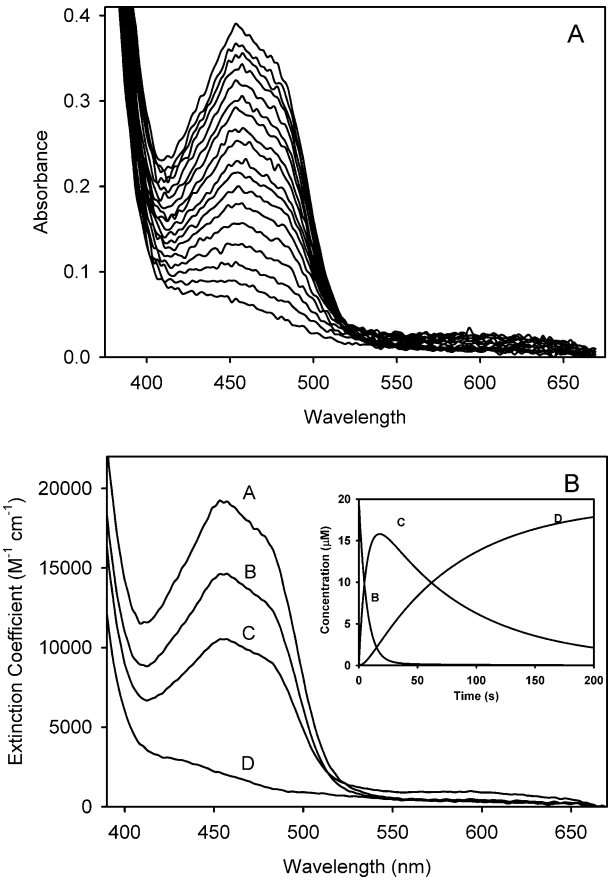

FIGURE 5: Reaction of MSR I22/L175 with NADPH followed by stopped-flow photodiode array spectroscopy. The conditions were as follows: 50 mM potassium phosphate buffer (pH 7.0) at 25 °C, [MSR I22/L175] = 25 μM, and [NADPH] = 500 μM. (A) Time-dependent spectral changes (recorded over 200 s) occurring upon rapid mixing of MSR I22/L175 with NADPH. The first spectrum was recorded 1.28 ms after mixing; only selected subsequent spectra are shown for purposes of clarity. (B) Deconvoluted spectra of the intermediates generated by global SVD analysis of the reaction depicted with spectra in panel A. The data (shown in panel A) were fitted globally to a reversible three-step A ↔ B ↔ C ↔ D model. The calculated rate constants (in s^{-1}) for this kinetic scheme are presented in Table 3. The inset shows calculated concentration profiles (over 200 s) of intermediates in the reaction of MSR 122/L175 with NADPH. Profiles were obtained by fitting the data shown in panel A to the reversible kinetic scheme (A ↔ B ↔ C ↔ D).

are shown in Figure 6. Over a time interval of 10 s, the observed rate constants determined from these measurements concur with the deconvoluted rate constants for the interconversion of spectral intermediates A → B and B → C in the photodiode array experiments (Table 3). The larger rate

Scheme 1

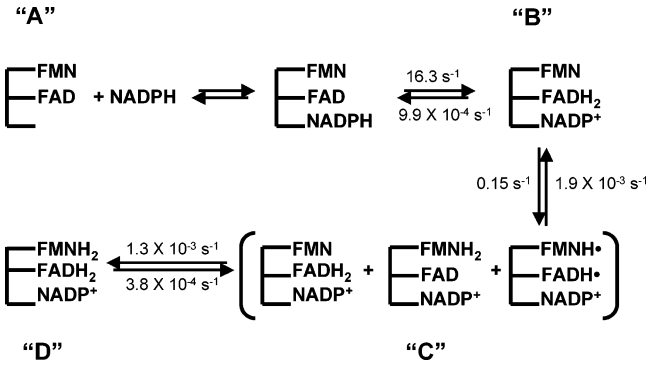

constant k_{obs1} exhibited a hyperbolic dependence on NADPH concentration (Figure 6B). A fit of the data to eq 5 gave a k_{lim} (maximal rate of flavin reduction) of 21.5 ± 0.2 and 20.5 ± 0.2 s^{-1} for MSR I22/L175 and MSR M22/S175, respectively, which are similar to the value for wild-type MSR I22/S175 (24.8 ± 0.3 s^{-1}). The data indicate that the small changes measured for the midpoint potential for the FAD_{ox}/FAD_{hq} potentials (and hence driving force for electron transfer between NADPH and the flavin) between wild-type and polymorphic variants do not influence the electron transfer kinetics to any degree that is significant to the cellular roles of the enzyme. The corresponding K values were 91.0 ± 3.1 and 74.4 ± 2.9 μM for MSR I22/L175 and M22/S175, respectively.

Stopped-flow absorption studies at 600 nm were also performed to characterize in more detail the small absorption changes at this wavelength observed by photodiode array spectroscopy. Single-wavelength experiments were performed by mixing MSR I22/L175 with a 20-fold excess of NADPH. The recorded transients displayed a rapid increase in absorption at 600 nm, followed by a decay of the signal over a longer period of time (Figure 7). The rate constants for the two kinetic phases were estimated from fitting the data to eq 4. The values obtained for k_{obs1} (130 s^{-1}) and k_{obs2} (13 s^{-1}) most likely represent the formation and decay of a charge transfer species, respectively, as described for the wild-type enzyme (*29*) and are similar in value ($k_{obs1} = 100$ s^{-1} and $k_{obs2} = 20$ s^{-1}, respectively). As with wild-type MSR, over an extended time base the absorbance increases again as the distribution of enzyme species relaxes to its most thermodynamically stable state.

Tryptophan fluorescence-monitored stopped-flow spectroscopy was also employed to investigate hydride transfer in MSR I22/L175. On the basis of structural analogies with

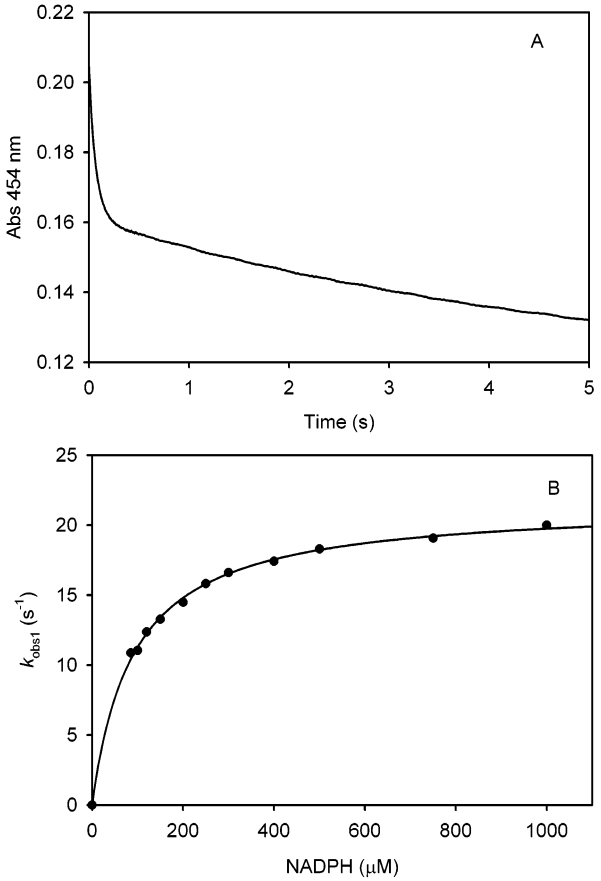

FIGURE 6: Single-wavelength absorption (454 nm) transient for the reaction of MSR I22/L175 with NADPH. The conditions were as follows: 50 mM potassium phosphate buffer (pH 7.0) at 25 °C, [MSR I22/L175] = 10 μM, and [NADPH] = 1000 μM. (A) Biphasic absorption trace for the reduction of MSR I22/L175. Fitting the data in panel A to eq 3 over 10 s yielded the following rate constant values: $k_{obs1} = 19.3\ s^{-1}$ and $k_{obs2} = 0.1\ s^{-1}$. (B) Dependence of k_{obs1} on NADPH concentration. The data in panel B were fitted to eq 3 to give the following: $k_{lim} = 21.5 \pm 0.2\ s^{-1}$ and $K = 91.0 \pm 3.1\ \mu$M.

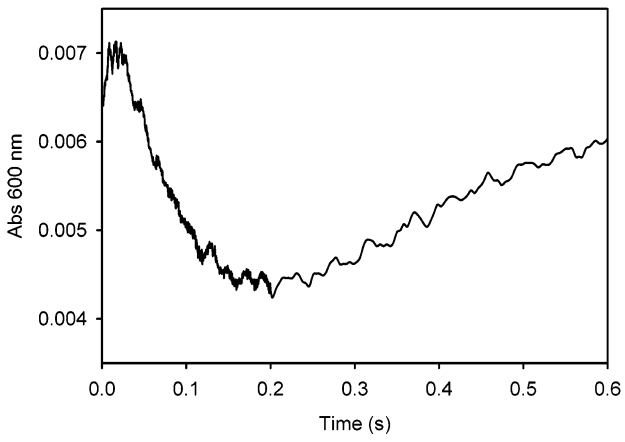

FIGURE 7: Single-wavelength absorption (600 nm) transient for the reaction of MSR I22/L175 with NADPH. The conditions were as follows: 50 mM potassium phosphate buffer (pH 7.0) at 25 °C, [MSR I22/L175] = 10 μM, and [NADPH] = 200 μM. The stopped-flow data were fitted to eq 4 and yielded the following rate constant values: $k_{obs1} = 130\ s^{-1}$ (for the up phase) and $k_{obs2} = 13\ s^{-1}$ (for the down phase).

rat liver CPR (*10*), tryptophan 697 is predicted to cover the *re*-face of the FAD isoalloxazine ring and move away from the ring upon transfer of hydride from NADPH. This

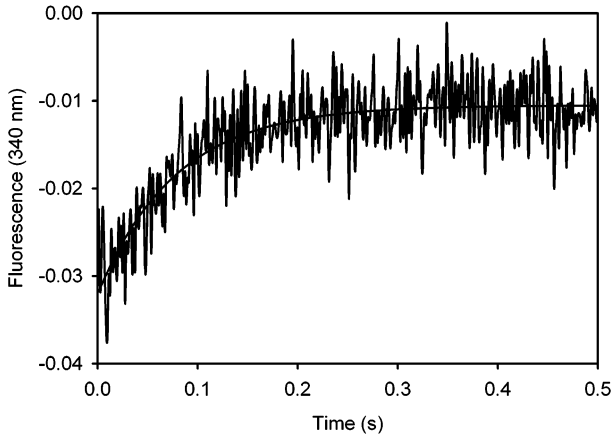

FIGURE 8: Tryptophan fluorescence transient for the reaction of MSR I22/L175 with NADPH. The conditions were as follows: 50 mM potassium phosphate buffer (pH 7.0) at 25 °C, [MSR I22/L175] = 10 μM, [NADPH] = 200 μM, excitation at 295 nm, and emission at 340 nm. The stopped-flow data were fitted to a single-exponential equation ($k_{obs1} = 15\ s^{-1}$).

concerted motion is accompanied by a change in fluorescence intensity, which can then be used to characterize the kinetics of hydride transfer, as demonstrated with wild-type MSR (*29*). Mixing of MSR I22/L175 with a 20-fold excess of NADPH generates a monophasic fluorescence transient, which can be fit to a single-exponential equation to give a k_{obs} rate constant of $15\ s^{-1}$ (Figure 8). This is consistent with the large k_{obs1} obtained from single-wavelength spectroscopy at 454 nm, under the same conditions.

DISCUSSION

Pathogenic mutations mapping to the genes involved in homocysteine metabolism, such as methionine synthase and MSR, impede transmethylation of homocysteine to methionine and result in hyperhomocysteinemia. Elevated homocysteine levels are associated with an increased risk for a variety of pathologies, including atherosclerosis (*30*), neural tube defects (*31*), and Alzheimer's disease (*32*−*34*). A collection of MSR mutants, consisting of deletions, insertions, and missense and nonsense mutations, have been identified throughout the MSR coding sequence (*2*, *21*). In addition to these mutants, which have pathogenic consequences (*11*, *16*, *35*), two common polymorphic variants in MSR have also been described (*21*, *23*). The first, I22M, has an isoleucine allele frequency of ∼0.55 in several populations (*18*, *21*, *22*) and may be a risk factor for Down's syndrome (*19*, *20*, *36*), neural tube defects (*21*, *37*), and premature coronary artery disease (*17*). The second polymorphism, S175L, was described in a homocystinuric *cbl*E patient, in conjunction with two other mutations, 1459G>A and 1623−1624insA (*23*), and a serine allele frequency of 0.62 was reported in a small control population.

We had previously evaluated the relative efficacies of the polymorphic versus the wild-type MSR variants in reductive activation of methionine synthase (*24*). We observed that with the variants, a 3−4-fold increase in the stoichiometry for MSR to methionine synthase was required for full activation. In this study, we have compared thermodynamic and kinetic properties of the MSR variants with those of wild-type MSR I22/S175 (*25*, *29*). The I22M variant is in the predicted FMN binding domain, whereas the S175L variant is predicted to reside in the interdomain linker region.

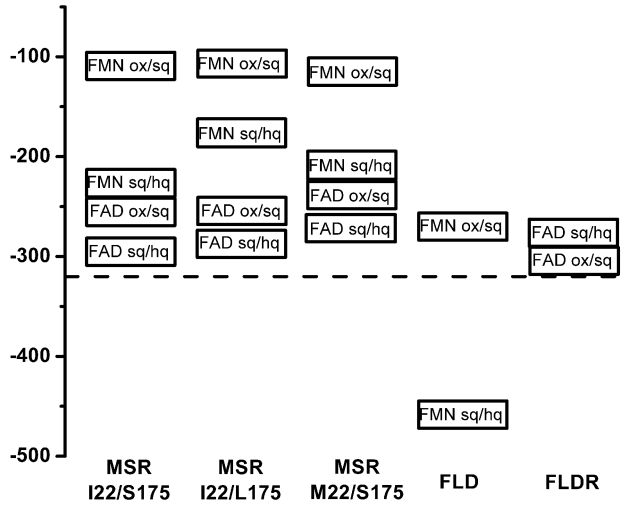

FIGURE 9: Comparison of flavin reduction potentials in MSR polymorphic variants and homologous bacterial flavoenzymes. The various midpoint potentials for the oxidized/semiquinone and semiquinone/hydroquinone couples of the FMN and FAD cofactors in human and *E. coli* methionine synthase-activating flavoenzymes (flavodoxin and flavodoxin reductase) are shown. These are MSR I22/S175 (*25*), MSR I22/L175 and MSR M22/S175 (this work; potentials shown are those from the fit of the 450−460 nm data to eq 2), flavodoxin (FLD), and flavodoxin reductase (FLDR) (*43*). The midpoint reduction potential for the physiological reductant NAD(P)H (−336 mV) is shown as a dashed line.

Anaerobic redox titrations of the two variants confirmed that both flavins generate blue, neutral semiquinone species, in agreement with results from EPR and UV−visible spectroscopy (*24*). The four midpoint potentials of the flavin cofactors in the two MSR variants were generally very similar to those of the wild-type protein (Figure 9). In addition, they fall within the range found in other diflavin reductases, with the major difference being that the redox couples in MSR are more closely disposed than in the other human dual flavoenzymes (CPR, NOS, and NR1). The highest midpoint potential is assigned to the FMN_{ox}/FMN_{sq} couple, which is considerably more positive than the remaining three potentials. In the two MSR variants studied here, the FMN_{ox}/FMN_{sq} potentials are (from 450 to 460 nm data fit to eq 2, unless otherwise stated) −103 mV (I22/L175) and −114 mV (M22/S175), which are similar to that of the wild-type MSR I22/L175 enzyme (−109 mV) and ∼25−35 mV more positive than that of NR1 (*38*) and ∼50−60 mV more negative than those of human CPR and NOS (*27*, *28*). The FMN_{sq}/FMN_{hq} and FAD_{ox}/FAD_{sq} couples are closely disposed, as in the other human enzymes containing both these flavin cofactors. However, there is a rather larger difference between the couples for the I22/L175 variant (77 mV) than for the wild type and the M22/S175 variant (27 and 24 mV, respectively). In wild-type and mutant isoforms, the order of the potentials is the same (FMN_{ox}/FMN_{sq} > FMN_{sq}/FMN_{hq} > FAD_{ox}/FAD_{sq} > FAD_{sq}/FAD_{hq}). Finally, the midpoint potential for the two-electron reduction of the FAD quinone to its hydroquinone is approximately −269 mV in the I22/L175 variant and −250 mV in the M22/S175 variant, compared with −273 mV for the wild-type. In all cases, the potentials are considerably more positive than that for the physiological reductant NADPH (midpoint potential of −336 mV), which favors electron transfer in the physiologically relevant direction. The situation is similar in neuronal NOS, but the corresponding redox couples for human CPR and NR1, and for P450 BM3, are very similar to that for the NADPH midpoint potential. In NR1, electron transfer between NADPH and FAD occurs at a rate of only $\sim 1\ s^{-1}$. However, in P450 BM3, the corresponding rate is several hundred-fold faster. Thus, it is difficult to correlate the rate of NADPH-dependent flavin reduction directly with the relative thermodynamic driving force in these systems. Clearly, there is considerable overlap in the midpoint potentials of the individual redox couples in all human diflavoenzymes, with subtle differences having evolved in each reductase to fulfill the catalytic requirements of the individual system.

The similarities in the thermodynamic properties of the wild type and polymorphic variants of MSR support a common mechanism for electron transfer to methionine synthase (Scheme 1). The first step, i.e., hydride transfer from NADPH to FAD, is followed by a disproportionation of the electrons between the flavins. Since the midpoint potential for the FMN_{ox}/FMN_{sq} couple is ∼70−120 mV more positive than the other three potentials, reduction of the FMN cofactor is greatly favored. The FMN hydroquinone presumably transfers an electron to the cob(II)alamin cofactor of methionine synthase. However, as discussed below, the redox potentials of the donor/acceptor pair are thermodynamically unfavorable for reduction of cob(II)alamin.

The cob(II)alamin/cob(I)alamin couple in solution has a very low redox potential of −610 mV at pH 7.0 (*39*), but the potential is shifted to −526 mV in the *E. coli* methionine synthase (*39*). The midpoint potentials for the semiquinone and hydroquinone forms of flavodoxin (the proximal reducing partner of bacterial methionine synthase) are −260 and −440 mV, respectively (*40*), which makes reduction of enzyme-bound cob(II)alamin a thermodynamically unfavorable reaction. However, the reduction reaction is facilitated by adoption of two strategies. First, association of flavodoxin with inactive methionine synthase results in a conformational change in the cob(II)alamin and leads to dissociation of the lower axial histidine ligand (*41*). In this base-off conformation, the reduction potential of the cob(II)alamin/cob(I)alamin couple is expected to be more positive. Second, rapid methylation of cob(I)alamin by *S*-adenosylmethionine serves to couple the endergonic reduction to an exergonic and irreversible methylation reaction and drives the reaction in the forward direction (*42*).

The flavin midpoint potentials reported in this study for the two MSR variants and previously for the wild-type I22/S175 protein (*25*) are more positive than for flavodoxin (*42*). They also differ, although to a lesser extent, from the flavin midpoint potentials in *E. coli* flavodoxin reductase (Figure 9) (*43*). Instead, they show redox properties more similar to those observed for the other eukaryotic reductases containing both FMN and FAD cofactors, to which they are evolutionarily much closer. Nevertheless, we expect human MSR utilizes a similar kinetic coupling strategy for activating methionine synthase, i.e., by reductive methylation, to facilitate electron transfer in the physiologically relevant direction between MSR and methionine synthase.

The similarity in the redox properties of the wild-type and polymorphic variants of MSR is reflected in the similarities in their electron transfer kinetics. The time-resolved spectra for the variants fit the same three-step kinetic model proposed

for wild-type MSR (Scheme 1). The rates at which the intermediates form and decay are comparable for the two polymorphic variants and match closely those found with the wild-type I22/S175 enzyme (Table 3). Thus, the overall behavior of the MSR polymorphic variants is similar to that of wild-type MSR in terms of the limiting rates of hydride transfer and the hyperbolic dependence of the flavin reduction rate on NADPH concentration (*29*).

The current study reveals that there are subtle changes in the redox properties of the flavin cofactors (particularly the FMN) in the polymorphic variants. However, in view of these minor changes in potential being relatively small in comparison with the large thermodynamic barrier faced with regard to electron transfer to methionine synthase, they are unlikely to have any considerable effect on this process *in vivo*. This prediction is borne out by the similarity in the transient kinetic behavior of the wild-type and mutant MSR enzymes demonstrated in this study. Thus, the data presented here suggest that the mutations do not have effects on flavin potentials or electron transfer kinetics that would impinge on the catalytic efficiency of the variants. In contrast, the polymorphic variants presumably differ from the wild-type I22/S175 enzyme in their affinity for their redox partner, methionine synthase, and are 3−4-fold less efficient. Together, these data provide a framework for characterization of mutations in MSR, particularly those associated with a homocystinuric phenotype in the *cbl*E complementation group (*14*, *23*, *35*).

REFERENCES

1. Olteanu, H., and Banerjee, R. (2001) *J. Biol. Chem. 276*, 35558−35563.
2. Leclerc, D., Wilson, A., Dumas, R., Gafuik, C., Song, D., Watkins, D., Heng, H. H. Q., Rommens, J. M., Scherer, S. W., Rosenblatt, D. S., and Gravel, R. A. (1998) *Proc. Natl. Acad. Sci. U.S.A. 95*, 3059−3064.
3. Iyanagi, T., and Mason, H. S. (1973) *Biochemistry 12*, 2297−2308.
4. Hevel, J. M., White, K. A., and Marletta, M. A. (1991) *J. Biol. Chem. 266*, 22789−22791.
5. Mayer, B., John, M., Heinzel, B., Werner, E. R., Wachter, H., Schultz, G., and Bohme, E. (1991) *FEBS Lett. 288*, 187−191.
6. Paine, M. J., Garner, A. P., Powell, D., Sibbald, J., Sales, M., Pratt, N., Smith, T., Tew, D. G., and Wolf, C. R. (2000) *J. Biol. Chem. 275*, 1471−1478.
7. Narhi, L. O., and Fulco, A. J. (1986) *J. Biol. Chem. 261*, 7160−7169.
8. Ostrowski, J., Barber, M. J., Rueger, D. C., Miller, B. E., Siegel, L. M., and Kredich, N. M. (1989) *J. Biol. Chem. 264*, 15796−15808.
9. Porter, T. D., and Kasper, C. B. (1986) *Biochemistry 25*, 1682−1687.
10. Wang, M., Roberts, D. L., Paschke, R., Shea, T. M., Masters, B. S. S., and Kim, J.-J. (1997) *Proc. Natl. Acad. Sci. U.S.A. 94*, 8411−8416.
11. Watkins, D., and Rosenblatt, D. S. (1989) *Am. J. Med. Genet. 34*, 427−434.
12. Rosenblatt, D. S. (1995) *Inherited disorders of folate transport and metabolism*, McGraw-Hill, New York.
13. Shevell, M. I., and Rosenblatt, D. S. (1992) *Can. J. Neurol. Sci. 19*, 472−486.
14. Wilson, A., Leclerc, D., Rosenblatt, D. S., and Gravel, R. A. (1999) *Hum. Mol. Genet.*, 2009−2016.
15. Watkins, D., and Rosenblatt, D. S. (1988) *J. Clin. Invest. 81*, 1690−1694.
16. Steen, C., Rosenblatt, D. S., Scheying, H., Braeuer, H. C., and Kohlschutter, A. (1997) *J. Inherited Metab. Dis. 20*, 705−706.
17. Brown, C. A., McKinney, K. Q., Kaufman, J. S., Gravel, R. A., and Rozen, R. (2000) *J. Cardiovasc. Risk 7*, 197−200.
18. Gaughan, D. J., Kluijtmans, L. A., Barbaux, S., McMaster, D., Young, I. S., Yarnell, J. W., Evans, A., and Whitehead, A. S. (2001) *Atherosclerosis 157*, 451−456.
19. Hobbs, C. A., Sherman, S. L., Yi, P., Hopkins, S. E., Torfs, C. P., Hine, R. J., Pogribna, M., Rozen, R., and James, S. J. (2000) *Am. J. Hum. Genet. 67*, 623−630.
20. O'Leary, V. B., Parle-McDermott, A., Molloy, A. M., Kirke, P. N., Johnson, Z., Conley, M., Scott, J. M., and Mills, J. L. (2002) *Am. J. Med. Genet. 107*, 151−155.
21. Wilson, A., Platt, R., Wu, Q., Leclerc, D., Christensen, B., Yang, H., Gravel, R. A., and Rozen, R. (1999) *Mol. Genet. Metab. 67*, 317−323.
22. Rady, P. L., Szucs, S., Grady, J., Hudnall, S. D., Kellner, L. H., Nitowsky, H., Tyring, S. K., and Matalon, R. K. (2002) *Am. J. Med. Genet. 107*, 162−168.
23. Zavad'akova, P., Fowler, B., Zeman, J., Suormala, T., Pristoupilova, K., and Kozich, V. (2002) *J. Inherited Metab. Dis. 25*, 461−476.
24. Olteanu, H., Munson, T., and Banerjee, R. (2002) *Biochemistry 41*, 13378−13385.
25. Wolthers, K. R., Basran, J., Munro, A. W., and Scrutton, N. S. (2003) *Biochemistry 42*, 3911−3920.
26. Dutton, P. L. (1978) *Methods Enzymol. 54*, 411−435.
27. Munro, A. W., Noble, M. A., Robledo, L., Daff, S. N., and Chapman, S. K. (2001) *Biochemistry 40*, 1956−1963.
28. Noble, M. A., Munro, A. W., Rivers, S. L., Robledo, L., Daff, S. N., Yellowlees, L. J., Shimizu, T., Sagami, I., Guillemette, J. G., and Chapman, S. K. (1999) *Biochemistry 38*, 16413−16418.
29. Wolthers, K. R., and Scrutton, N. S. (2004) *Biochemistry 43*, 490−500.
30. Refsum, H., Ueland, P. M., Nygard, O., and Vollset, S. E. (1998) *Annu. Rev. Med. 49*, 31−62.
31. Mills, J. L., McPartlin, J. M., Kirke, P. N., Lee, Y. J., Conle, M. R., and Weir, D. G. (1995) *Lancet 345*, 149−151.
32. Seshadri, S., Beiser, A., Selhub, J., Jacques, P. F., Rosenberg, I. H., D'Agostino, R. B., Wilson, P. W., and Wolf, P. A. (2002) *N. Engl. J. Med. 346*, 476−483.
33. Miller, J. W. (1999) *Nutr. Rev. 57*, 126−129.
34. Clarke, R., Smith, A. D., Jobst, K. A., Refsum, H., Sutton, L., and Ueland, P. M. (1998) *Arch. Neurol. 55*, 1449−1455.
35. Vilaseca, M. A., Vilarinho, L., Zavadakova, P., Vela, E., Cleto, E., Pineda, M., Coimbra, E., Suormala, T., Fowler, B., and Kozich, V. (2003) *J. Inherited Metab. Dis. 26*, 361−369.
36. Bosco, P., Gueant-Rodriguez, R. M., Anello, G., Barone, C., Namour, F., Caraci, F., Romano, A., Romano, C., and Gueant, J. L. (2003) *Am. J. Med. Genet. 121A*, 219−224.
37. Gueant-Rodriguez, R. M., Rendeli, C., Namour, B., Venuti, L., Romano, A., Anello, G., Bosco, P., Debard, R., Gerard, P., Viola, M., Salvaggio, E., and Gueant, J. L. (2003) *Neurosci. Lett. 344*, 189−192.
38. Finn, R. D., Basran, J., Roitel, O., Wolf, R. C., Munro, A. W., Paine, M. J. I., and Scrutton, N. S. (2003) *Eur. J. Biochem. 270*, 1−12.
39. Banerjee, R. V., Harder, S. R., Ragsdale, S. W., and Matthews, R. G. (1990) *Biochemistry 29*, 1129−1137.
40. Hoover, D. M., Jarrett, J. T., Sands, R. H., Dunham, W. R., Ludwig, M. L., and Matthews, R. G. (1997) *Biochemistry 36*, 127−138.
41. Jarrett, J. T., Huang, S., and Matthews, R. G. (1998) *Biochemistry 37*, 5372−5382.
42. Fujii, K., Galivan, J. H., and Huennekens, F. M. (1977) *Arch. Biochem. Biophys. 178*, 662−670.
43. McIver, L., Leadbeater, C., Campopiano, D. J., Baxter, R. L., Daff, S. N., Chapman, S. K., and Munro, A. W. (1998) *Eur. J. Biochem. 257*, 577−585.

BI035910I